Intercalation Induced Reversible Electrochromic Behavior of Two-dimensional $Ti_3C_2T_x$ MXene in Organic Electrolytes

Jianmin Li,[#a, b] Xuehang Wang,[#a] Weiwei Sun,[#c, d] Kathleen Maleski,[a] Christopher E. Shuck,[a] Ke Li,[a] Patrick Urbankowski,[a] Kanit Hantanasirisakul,[a] Xiaofeng Wang,[a] Paul Kent,[c, e] Hongzhi Wang,[b] Yury Gogotsi*[a]

Y. G., P. K. and H. W. supervised the project. J. L., X. W. performed the characterizations, K. L. synthesized $Ti_3C_2T_x$, C. S., K. H., P. U. and X. W. performed *in-situ* XRD, *in-situ* UV-vis, XPS and structure measurements, respectively. W. S. performed DFT simulations. J. L., X. W., W. S. and K. M. wrote the manuscript. All authors have given approval to the final version of the manuscript.
# These authors contributed equally.

[a] Dr. Jianmin Li, Dr. Xuehang Wang, Dr. Kathleen Maleski, Dr. Christopher E. Shuck, Dr. Ke Li, Dr. Patrick Urbankowski, Mr. Kanit Hantanasirisakul, Prof. Xiaofeng Wang, Prof. Yury Gogotsi
A.J. Drexel Nanomaterials Institute and Department of Materials Science and Engineering
Drexel University
Philadelphia, PA 19104, USA
E-mail: gogotsi@drexel.edu
[b] Dr. Jianmin Li, Prof. Hongzhi Wang
State Key Laboratory for Modification of Chemical Fibers and Polymer Materials, College of Materials Science and Engineering
Donghua University
Shanghai 201620, PR China
[c] Dr. Weiwei Sun, Prof. Paul Kent
Center for Nanophase Materials Sciences
Oak Ridge National Laboratory
Oak Ridge, TN 37831, USA
[d] Prof. Weiwei Sun
SEU-FEI Nano-Pico Center, Key Laboratory of MEMS of Ministry of Education
Southeast University
Nanjing 210096, China
[e] Prof. Paul Kent
Computational Sciences and Engineering Division
Oak Ridge National Laboratory
Oak Ridge, TN 37831, USA

Supporting information for this article is given via a link at the end of the document.

Abstract: MXenes, a large family of two-dimensional materials, have attracted tremendous attention due to their unique physical and chemical properties. Reversible ion intercalation between MXene layers allows modification of the optical, thermal, magnetic, and chemical properties. The electrochemical charge/discharge of MXenes in aqueous electrolytes was reported to lead to reversible electrochromic behavior. In this work, the electrochromic effect of semitransparent $Ti_3C_2T_x$ MXene film was probed by electrochemical intercalation of Li ions. Correspondingly, a peak shift of 100 nm was observed in the UV-vis spectrum. By combining *in-situ* Raman spectroscopy, *in-situ* X-ray diffraction, and density functional theory calculations, we show that the electrochromic shift is primarily due to the formation of robust O-Li bonds and the emerging bands induced changes of inter-band excitations. Understanding the mechanism of electrochromic behavior in $Ti_3C_2T_x$ lay the foundations of designating 2D materials with durable, controllable, and efficient intercalation-induced electrochromic behaviors.

Introduction

Electrochromism, the change of color by application of a potential to specific electrode materials, is a widely used phenomenon in light-regulation and displays.[1] Typically, electrochromic behavior is the result of redox reactions under an applied electric field, and the color change is faster than thermochromism or photochromism, where the active material changes color when experiencing temperature changes or exposed to electromagnetic radiation.[1b, 2] Alteration of the redox state of organic materials, such as polymers[3] and some organic molecules [2b, 4], leads to color change (e.g., polyaniline, polypyrrole and viologens). However, most organic materials are sensitive to UV light (<400 nm) and bleach in the near-infrared region. This limits their practical applications as smart windows, for example. Other functional materials, such as conducting oxides, make use of the surface plasmonic effects, delivering electrochromic performance with rapid switching speed and great durability, however, their surface plasmon resonance only occurs in the mid to near-infrared region.[5] In comparison, the electrochromic effect introduced by reversible ion intercalation into transition metal oxides (TMOs), shows color change in the visible region. For example, WO_3 shows the change in color from dark blue to transparent after the intercalation of electrolyte ions [6], but low conductivity of the oxide requires the use of an additional layer of transparent conductor, such as intdium-tin oxide (ITO).

The electrochromic behavior is usually induced by the injection of charge, which is realized by the intercalation of protons or alkali ions.[2a, 7] Intercalation or deintercalation of ions

into/out of bulk TMOs can induce reversible electrochromic effects, and is accompanied by charge storage during cycling.[8] However, the electrochromic effect in bulk TMOs shows low durability and coloration efficiency, because the process is diffusion-controlled and is often limited by material degradation or phase changes.[7b, 8a] Alternatively, intercalation of ions into thin films fabricated from 2D materials differs greatly compared to the intercalated bulk materials. In many cases, the differences can result in drastically improved device performance for a wide range of applications, such as energy storage, magnetic properties, as well as electrochromic performance.[9] Assuming a given 2D material in the format of thin film can be operated under low resistance and highly reversible intercalation, accompanied by redox reactions, it should be able to act as an ideal electrochromic material.

2D transition metal carbides and/or nitrides, termed MXenes, mostly have metallic conductivity, hydrophilic surfaces, high mechanical strength, and are promising redox-active intercalation hosts.[10] With a metal carbide core and transition metal oxide surface, MXene electrodes show charge storage capability with fast charge/discharge speed.[11] Titanium carbide, $Ti_3C_2T_x$ (T_x stands for the surface terminations, including =O, -OH and -F), exhibiting outstanding electronic, optical, mechanical, and thermal properties, was found to show electrochromic behavior in an acidic electrolyte during cycling under negative potential.[12] However, the relationship between the intercalation process and the color change reflected in the electrochromic behavior is still not fully understood and lacking in-depth investigations.

In this work, the electrochromic behavior of $Ti_3C_2T_x$ thin films was investigated in organic electrolytes cycling with Li^+ and 1-ethyl-3-methyl-imidazolium ($EMIM^+$) ions. The organic electrolyte is used to avoid corrosive acidic electrolytes and achieve a larger operating voltage window. The intercalation of Li ions from 1M LiTFSI in propylene carbonate (PC) into $Ti_3C_2T_x$ leads to electrochromic behavior dominated by pseudocapacitive intercalation. In addition, *in-situ* X-ray diffraction (XRD) and *in-situ* Raman spectroscopy were used to show that the surface groups are highly correlated with the intercalation-induced electrochromic behavior. Density functional theory (DFT) calculations indicate that the =O and -OH terminated MXenes result in varying binding mechanisms ultimately leading to distinct band excitations. We thus demonstrate that the electrochromic phenomenon resulting from Li intercalation is predominantly driven by the O-termination.

Results and Discussion

The suspension of monolayer $Ti_3C_2T_x$ MXene (Figure 1a) was prepared following the previously reported approach as described in Experimental Section.[13] A typical scanning electron microscope (SEM) image of the monolayer $Ti_3C_2T_x$ flakes obtained from the suspension is presented in Figure S1a, from which the lateral dimension of the flakes is generally in the range of 200-300 nm. The semitransparent $Ti_3C_2T_x$ thin film was prepared by spray coating the colloidal solution of delaminated $Ti_3C_2T_x$ with the concentration of ~2 mg mL^{-1} onto a glass substrate (see Figure 1a), where the thickness was controlled by the number of spray coating passes. The SEM images (see Figure S2) show that the $Ti_3C_2T_x$ film that showed a transmittance of about 60% at 550 nm is uniform with a thickness of ~50 nm. Raman spectroscopy was conducted to understand the surface environment (Figure S3). According to a prior DFT study,[14] the Raman peaks at 200 and 723 cm^{-1} are correspondingly assigned to the Ti−C and C−C vibrations (A_{1g} symmetry) of the oxygen terminated $Ti_3C_2O_2$. The peak at 620 cm^{-1} is primarily resulting from E_g vibrations of the C atoms in the OH-terminated $Ti_3C_2T_x$. The peaks at 389 and 580 cm^{-1} are attributed to the E_g and A_{1g} vibrations of the O atoms, respectively. The 282 cm^{-1} peak appears due to the contribution of H atoms in the OH groups of $Ti_3C_2T_x$.

A three-electrode cell was assembled by using the $Ti_3C_2T_x$ coated glass slide ($Ti_3C_2T_x$-glass) as the working electrode, ITO coated glass (ITO-glass) as the counter electrode, a silver wire as the reference electrode, and the cell was filled with different organic electrolytes for the *in-situ* tests, as shown in Figure 1b, c. Furthermore, digital images of the assembled cell tested in 1M LiTFSI/PC electrolyte in Figure 1d showed a reversible green-to-blue color change as the applied voltage changed from 0 to -2 V, indicating the electrochromic behavior of $Ti_3C_2T_x$ MXene. The RGB values were collected at the central point using Adobe Photoshop CS6. The digital video shown in Video S1 was filmed during cyclic voltammetry (CV) scanning at a scan rate of 10 mV s^{-1} between -2 and 0.2 V to demonstrate the electrochromic performance of $Ti_3C_2T_x$ MXene. The color switched from green to blue gradually and returned to green as the CV was scanned back to 0 V, conforming the reversible color-changing process.

To quantify the color changes of the $Ti_3C_2T_x$ film in LiTFSI/PC, the optical properties were evaluated by combining the cyclic voltammetry with ultraviolet-visible (UV–vis) spectrophotometry. The UV-vis data was collected at different potentials during the CV test in a stable potential window (-2 to 0.2 V) at 2 mV s^{-1} (Figure 2a). As shown in Figure 2b and Figure S4, the device has an initial transmittance of 57% at a trough (*T*) at 780 nm, a crest at 550 nm (*C1*) a transmittance of 64% and a shoulder at 428 nm (*S*) with a transmittance of 53%. As the voltage increased from 0 to -2 V, a blue shift occurred on *T* and *C1*, accompanied by an increase in transmittance. It is worth noting that the crest (*C2*) due to the free-electron plasma oscillations, which is at about 1250 nm initially,[15] shifted to 929 nm with a transmittance of 68% when the voltage reached -1.5 V. This indicates that the peak shifts to higher energies when charge is injected. At -2 V, *T* shifted to 680 nm with a transmittance of 61%, demonstrating a blue shift of 100 nm and a 4% increase in transmittance, accompanying the visible green-to-blue color change. Moreover, *C1* shifted to 536 nm with 68% transmittance (4% increase), while *C2* shifted to 854 nm with the same transmittance. Additionally, the transmittance of *S* increased 8% without shifting. As the voltage was returned to OCV, the UV-vis curve returned to its initial state, indicating a reversible blue-to-green color change process (see Figure S5a). The coloration efficiency (CE) at 450 nm and 810 nm were calculated to be 7 and 6 cm^2 C^{-1} (Figure S6), respectively, at an applied voltage of -2 V.

The transmittance at 450 nm and 810 nm were selected to evaluate the cycle stability of the $Ti_3C_2T_x$ semitransparent film; the two characteristics were obtained by applying a pulse voltage of -2 and 0.2 V, repeating for 300 cycles, as shown in Figure S7a, b. Figure S7c shows 14 cycles in detail, which demonstrate the stable transmittance oscillation during electrochemical cycling, indicating the high electrochemical stability of $Ti_3C_2T_x$ in organic electrolytes. To further confirm its electrochemical stability, XRD patterns before and after long-term cycling were conducted and shown in Figure S8, showing no phase transformation or oxidation after cycling. *Ex situ* X-ray

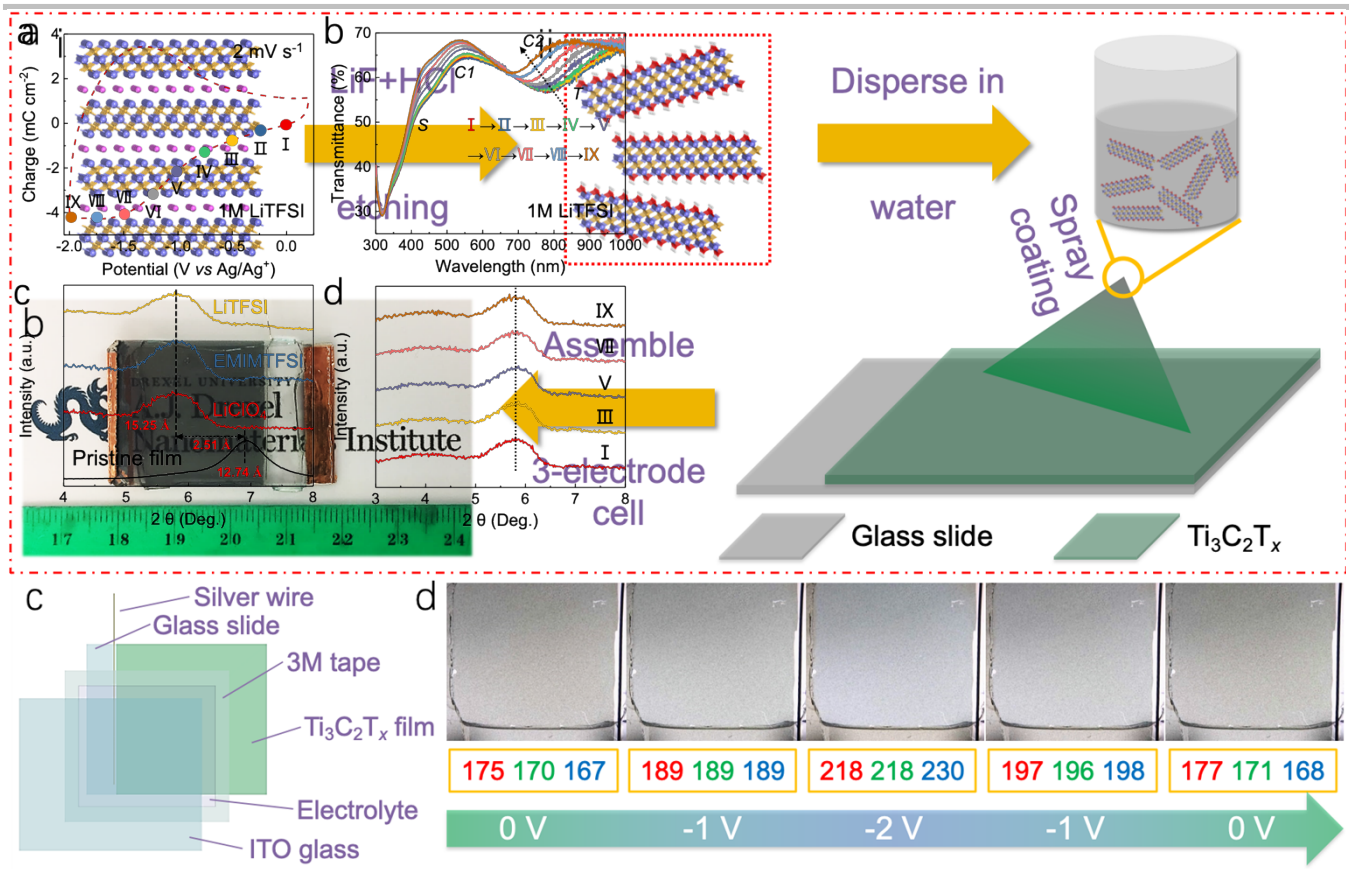

photoelectron spectroscopy (XPS) was used as an additional technique to confirm the stability of $Ti_3C_2T_x$ after 300 cycles (see Figure S9), which indicated that the state of $Ti_3C_2T_x$ was retained with only slight oxidization. The larger anodic potential in 1 M EMIMTFSI electrolyte may induce oxidation of the MXene film.

Figure 1. (a) Schematic illustration of a $Ti_3C_2T_x$ film prepared by spray coating. (i) and (ii) are the structure of Ti_3AlC_2 and $Ti_3C_2T_x$, where Ti, Al, C, O, and H atoms are shown in blue, purple, yellow, red, and white, respectively. Digital image (b) and schematic illustration (c) of the fabricated 3-electrode cell for *in-situ* testing. (d) Digital images of the device at different voltages in 1M LiTFSI electrolyte and their related red-green-blue (RGB) values.

The electrochromic behavior was measured in $Ti_3C_2T_x$ induced by intercalating protons within acidic aqueous electrolytes.[12] Recently, strong lithium intercalation of $Ti_3C_2T_x$ in organic solvent PC with a large voltage window was reported.[13] Similarly, such a significant color change of MXene in LiTFSI/PC electrolyte is expected to relate to the intercalation/deintercalation of Li ions during cycling. However, it is still unclear how the intercalation process is correlated to the optical change during cycling. As the intercalation process can physically expand or shrink the interlayer space, in addition to modification of the surface terminations, and bring about charge/electron transfer with MXene surface groups.[16]

Different intercalating ions are capable of changing the interlayer space because the ion size and interactions are different.[17] 1-Ethyl-3-methylimidazolium bis(trifluoromethyl-sulfonyl)imide (EMIMTFSI) in PC was chosen to test the electrochromic performance, as $EMIM^+$ (0.7 nm in length and 0.4 nm in width) is much larger than Li-ions. Previously, it was observed that a change in interlayer space modifies the optical transmission.[9a, 18] Larger ions may open up a greater interlayer space during cycling, which may be beneficial for electrochromic performance. However, *in-situ* UV-vis data for 1M EMIMTFSI/PC showed similarly reversible, but smaller electrochromic shift (see Figure S5b, c), with a stable potential window from -1.6 to 0.6 V. The *C2* didn't appear even when the applied voltage increased to -1.6 V. The blue shift for *T* and *C1* was 33 and 18 nm, displaying a transmittance change of 1% and 2%, respectively. Notably, almost no transmittance change was observed on the *S*, and therefore the intercalation of $EMIM^+$ does not lead to a more obvious transmission change during cycling.

To study the effect of the electrolyte further, 1M $LiClO_4$/PC electrolyte, which is a common electrolyte used in electrochromic devices, was used to reveal the effects of anion interactions on the interlayer space change and the electrochromic performance. The $Ti_3C_2T_x$ MXene electrode showed a stable potential window of -2 to 0.2 V when cycled in $LiClO_4$/PC, which is same with LiTFSI/PC. The *in-situ* UV-vis data in Figure S5d shows the optical response of $Ti_3C_2T_x$ in $LiClO_4$/PC. For *T*, a 39 nm blue shift was measured, with a 2% change in transmittance, while the *C1* showed a blue shift of 24 nm accompanied by a transmittance change of 3%. Interestingly, *C2* appeared at 982 nm with a transmittance of 67%, when the potential reached -0.5 V, and it shifted to 867 nm as the voltage

Figure 2. The cyclic voltammetry at the scan rate of 2 mV s^{-1} (a), the colored points show where the UV-vis and XRD data were collected. (b) *In-situ* UV-vis transmittance tests in 1M LiTFSI/PC electrolyte. (c) *In-situ* XRD study of the (002) peak of $Ti_3C_2T_x$ in different electrolytes. (d) *In-situ* XRD results collected at different voltages in 1M LiTFSI/PC electrolyte.

increased to -2.0 V, with the transmittance further increasing by 2%. Furthermore, a variation of about 4% in transmittance was observed for *S*, showing a synchronous behavior.

In-situ XRD was performed to understand how the interlayer space affects the optical properties during cycling. As shown in Figure 2c, the (002) peak of MXene was at 6.93° (d-spacing of 12.74 Å), indicating an interlayer space of 3.16 Å. After pre-cycling in these three electrolytes, the (002) peak shifted to 5.79° (d-spacing of 15.25 Å), indicating an interlayer spacing of 5.67 Å, which remains almost constant regardless of the applied voltage increased during testing. There is no shift or change of intensity for the (002) peak at different voltages (see Figure 2d), indicating that the interlayer space of $Ti_3C_2T_x$ flakes remains constant during the electrochemical reactions. This phenomenon also implies that cation intercalation may only occur in the first several cycles during the electrochemical test. Notably, a d-spacing of 15.25 Å is much larger than the size of Li or EMIM ions, indicating that the MXene interlayer has both solvent and intercalated ions. This might be because the thin spray-coated transparent film is more accessible to diffusion of ions. Such a large interlayer spacing with a solvent-rich environment explains the static nature of the interlayer space during cycling in all studied systems. Because the optical properties changed irrespective of the interlayer space, it stands to reason that the interlayer space has a minor impact on the electrochromic effect of MXenes.

The charge transfer, even if partial, that occurs following ion intercalation in MXenes, may also lead to the observed electrochromic effect and can contribute to the overall charge storage. The discharge capacities at 2 mV s^{-1}, calculated by integrating the anodic scans of the CV curves in Figure 3a, are 86.9 C g^{-1}, 44 C g^{-1} and 35 C g^{-1} in LiTFSI, $LiClO_4$ and

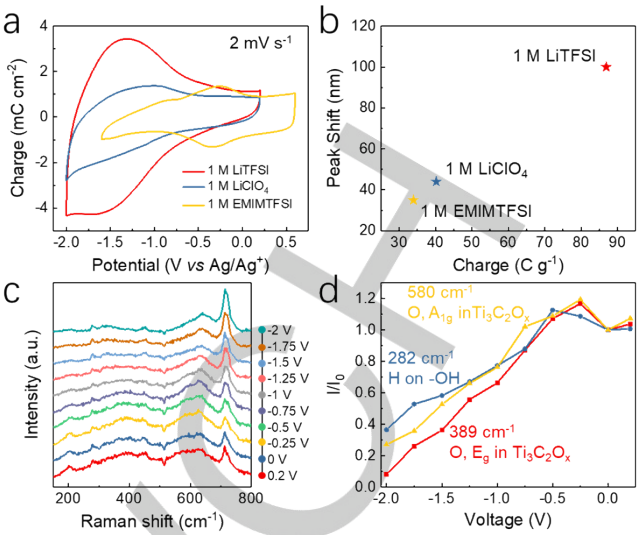

Figure 3. (a) Cyclic voltammetry curves of the $Ti_3C_2T_x$ film and (b) UV-vis peak shift versus the charge capacity recorded in different electrolytes. *In-situ* Raman spectra (c) and the statistics (d) of 282, 389 and 580 cm^{-1} peaks shift vs voltage for $Ti_3C_2T_x$ recorded in 1M LiTFSI/PC electrolyte.

EMIMTFSI-based electrolytes, respectively. We summarized their charge capacities and the corresponding peak shift of UV-vis spectrum in Figure 3b, where the optical shifts are positively correlated with the charge capacity.

To better understand the charge storage process for $Ti_3C_2T_x$ in 1M LiTFSI/PC, *in-situ* electrochemical Raman spectroscopy measurements were conducted to track the surface groups during cycling (see Figure 3c and Figure S10); from this, the voltage-dependent changes in Raman bands assigned to $Ti_3C_2T_x$ were recognized. Figure 3d shows the corresponding statistical data of the peak intensities at 282, 389 and 580 cm^{-1}, corresponding to the H atoms in the -OH groups, E_g and A_{1g} vibrational modes on O atoms, respectively. The intensity of the vibrations for H on -OH groups began decreasing when $Ti_3C_2T_x$ was charged to -0.5 V, which may be the onset of intercalated Li-ion binding with -OH groups. Then, it reached a minimum intensity of 36% at -2 V, corresponding to the fully charged state. As for the response of =O groups, the onset voltage of its vibrations starts to decrease at -0.25 V, which is smaller than for -OH. Notably, the E_g and A_{1g} modes of O atoms exhibited a decrease of 92% and 73%, respectively. Such results confirm that the interaction between Li ions and the O-terminated MXene surface is easier than with OH terminations, and the vibrations of O terminational groups are suppressed by Li intercalation.

To better understand how Li intercalation affects the observed optical transmittance at different applied potentials, we further performed DFT calculations, focusing on the band structure on the systems with different concentrations of Li intercalated into $Ti_3C_2O_2$ and $Ti_3C_2(OH)_2$. Due to large experimental d-spacing, and thus interlayer spacing, for $Ti_3C_2T_x$, DFT calculations were performed based on monolayer structure models.

The optical transmittance is obtained based on the most energetically favorable configuration for each Li concentration on purely =O and -OH terminated $Ti_3C_2T_x$. The intensity of transmittance shown in Figure 4 was determined by the reversed optical reflectivity derived from the dielectric function. Note that the transmission spectra of $Ti_3C_2(OH)_2Li_x$ ceases at x~1, because the intercalated Li atoms transition to physisorption on the hydroxyl terminated MXene at this concentration and above,

in contrast to $Ti_3C_2O_2Li_x$, where the Li atoms chemisorb on the surface up to full coverage. Thus, it is expected that the fully oxygen terminated MXene will become more transparent, because the chemical bonding will more significantly modify the band structure. In Figure 4b, an increase in the intensity of the optical transmission spectra correlates with Li content, and moreover, the transmittance peak shifts to higher energies up to ~2 eV (~620 nm), similar to what was observe for protons intercalation.[19] The intensity of the transmission spectra in the short wavelength regime is also gradually suppressed and experiences a slight blueshift in $Ti_3C_2(OH)_2Li_x$, which suggests that the observed electrochromic behavior primarily occurs on the O-terminated MXenes and is less contributed to by hydroxyl terminated MXene. Indeed, as shown by the band structures in Figure S12 and the charge transfer analysis in Table S1, Li states are emerging and hybridizing with the O-terminated MXene. They establish a new excitation path at ~2 eV. The emerging band excitations in turn cause the optical transmittance peak ~500-650 nm (1.9-2.5 eV), which agrees with the measurements in both the trends of wavelength shift as well as the intensity enhancement. This indicates that the electrochromic behavior is determined by the type of interaction between the intercalates and the MXene surface. The changes in band structure and charge transfer are well correlated with the presented transmittance in both intensity and the energetic shifts, and might be further modified in other MXenes or by different surface terminations.

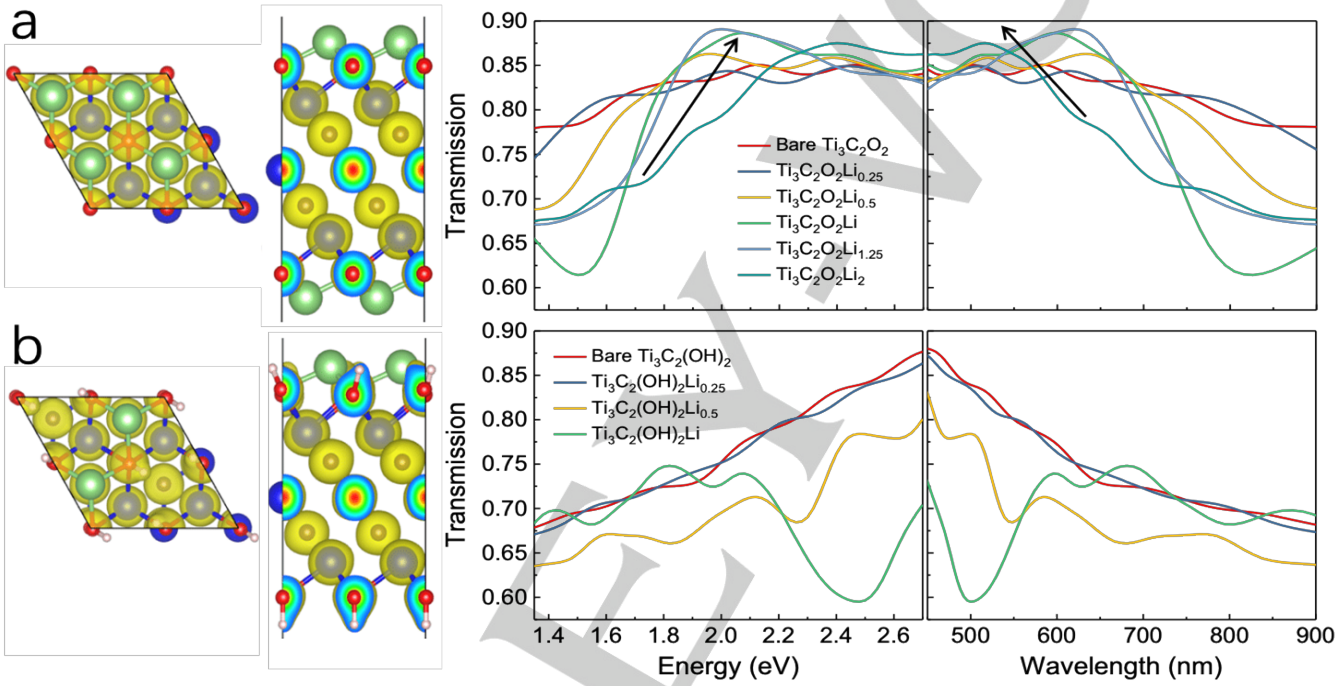

Figure 4. (a) The charge density of $Ti_3C_2O_2Li_2$ in both top and side view and computed optical transmission $Ti_3C_2O_2Li_x$ on energy and wavelength scales. (b) The charge density of $Ti_3C_2(OH)_2Li_2$ and calculated transmission of $Ti_3C_2(OH)_2Li_x$ on energy and wavelength scales. Note that the isosurface level is 0.1 e/Å^3. The atomic index of elements is Ti (blue), C (yellow), O (red), H (white) and the adsorbed Li atoms (green). The black arrows in (a) indicates the main peak shift with an increase of Li content.

Conclusion

The electrochromic effect of $Ti_3C_2T_x$ semitransparent films were observed while cycling in organic electrolytes. Three different salts (LiTFSI, EMIMTFSI, and $LiClO_4$) in propylene carbonate solvent were used to probe the mechanism of the electrochromic effect in $Ti_3C_2T_x$. *In-situ* Raman spectroscopy measurements indicated that the surface terminations (=O and -OH groups) varied during cycling. DFT calculations further confirm that the interactions between O-termination and the increasing number of Li atoms lead to charge transfer and directly alter the optical excitations, resulting in the transmission peak shift, and the theoretically predicted trend in transmission is in an excellent agreement with the experiments.

Acknowledgements

Acknowledgements Text. This research was supported by the Fluid Interface Reactions, Structures, and Transport (FIRST) Center, an Energy Frontier Research Center (EFRC) funded by the US Department of Energy, Office of Science, and Office of Basic Energy Sciences. J.L. thanks the support through the Special Excellent PhD International Visit Program by Donghua University. W.S. acknowledges the National Natural Science Foundation of China (Grant No. 51902052). K.M. thanks the support from the Army Research Office under Cooperative Agreement Number W911NF-18-2-0026 via the Surface Science Initiative Program (PE 0601102A Project VR9) at the Edgewood Chemical Biological Center. XRD, SEM, and XPS analyses were performed at the Centralized Research Facilities (CRF) at Drexel University. This research used resources of the National Energy Research Scientific Computing Center (NERSC), a U.S. Department of Energy Office of Science User Facility operated under Contract No. DE-AC02-05CH11231.

Keywords: MXene • Electrochromic • Photoelectronic • Organic electrolyte • Transparent device

[1] a) L. M. Loew, S. Scully, L. Simpson, A. S. Waggoner, *Nature* **1979**, *281*, 497-499; b) N. Elool Dov, S. Shankar, D. Cohen, T. Bendikov, K. Rechav, L. Shimon, M. Lahav, M. E. van der Boom, *J. Am. Chem. Soc.* **2017**, *139*, 11471-11481; c) C. M. Lampert, *Sol. Energy Mater. Sol. Cells* **1998**, *52*, 207-221; d) R. J. Mortimer, A. L. Dyer, J. R. Reynolds, *Displays* **2006**, *27*, 2-18; e) K. Takada, R. Sakamoto, S. Yi, S. Katagiri, T. Kambe, H. Nishihara, *J. Am. Chem. Soc.* **2015**, *137*, 4681-4689.

[2] a) W. Wu, M. Wang, J. Ma, Y. Cao, Y. Deng, *Adv. Electron. Mater.* **2018**, *4*, 1800185; b) J. Palenzuela, A. Viñuales, I. Odriozola, G. Cabañero, H. J. Grande, V. Ruiz, *ACS Appl. Mater. Inter.* **2014**, *6*, 14562-14567.

[3] a) A. Ghoorchian, F. Tavoli, N. Alizadeh, *J. Electroanal. Chem.* **2017**, *807*, 70-75; b) J. Li, A. Levitt, N. Kurra, K. Juan, N. Noriega, X. Xiao, X. Wang, H. Wang, H. N. Alshareef, Y. Gogotsi, *Energy Storage Mater.* **2019**, *20*, 455-461; c) G. Cai, P. Darmawan, M. Cui, J. Wang, J. Chen, S. Magdassi, P. S. Lee, *Adv. Energy Mater.* **2016**, *6*, 1501882.

[4] a) A. N. Woodward, J. M. Kolesar, S. R. Hall, N. Saleh, D. S. Jones, M. G. Walter, *J. Am. Chem. Soc.* **2017**, *139*, 8467-8473; b) H. Lu, S. Kao, H. Yu, T. Chang, C. Kung, K. Ho, *ACS Appl. Mater. Inter.* **2016**, *8*, 30351-30361; c) Y. Alesanco, A. Viñuales, G. Cabañero, J. Rodriguez, R. Tena-Zaera, *ACS Appl. Mater. Inter.* **2016**, *8*, 29619-29627.

[5] a) G. J. Stec, A. Lauchner, Y. Cui, P. Nordlander, N.J. Halas, *ACS Nano* **2017**, *11*, 3254-3261; b) T. Xu, E. C. Walter, A. Agrawal, C. Bohn, J. Velmurugan, W. Zhu, H. J. Lezec, A. A. Talin, *Nat. Commun.* **2016**, *7*, 10479; c) M. Atighilorestani, H. Jiang, B. Kaminska, *Adv. Opt. Mater.* **2018**, *6*, 1801179.

[6] a) G. Cai, M. Cui, V. Kumar, P. Darmawan, J. Wang, X. Wang, A. L. Eh, K. Qian, P. S. Lee, *Chem. Sci.* **2016**, *7*, 1373-1382; b) L. Santos, P. Wojcik, J. V. Pinto, E. Elangovan, J. Viegas, L. Pereira, R. Martins, E. Fortunato, *Adv. Electron. Mater.* **2015**, *1*, 1400002; c) X. Zhou, X. Zheng, B. Yan, T. Xu, Q. Xu, *Appl. Surf. Sci.* **2017**, *400*, 57-63.

[7] a) A. Azens, L. Kullman, G. Vaivars, H. Nordborg, C. Granqvist, *Solid State Ionics* **1998**, *113*, 449-456; b) R. C. Evans, A. Ellingworth, C. J. Cashen, C.R. Weinberger, J. B. Sambur, *P. Natul. Acad. Sci. USA* **2019**, *116*, 12666-12671.

[8] a) H. Qu, H. Zhang, X. Zhang, Y. Tian, B. Wang, X. Li, J. Zhao, Y. Li, *J. Mater. Sci.* **2017**, *52*, 11251-11268; b) F. Lin, D. Nordlund, T. Weng, R. G. Moore, D. T. Gillaspie, K. M. Jones, A. C. Dillon, R. M. Richards, C. Engtrakul, *Adv. Mater. Interfaces* **2015**, *2*, 1400523.

[9] a) W. Bao, J. Wan, X. Han, X. Cai, H. Zhu, D. Kim, D. Ma, Y. Xu, J. N. Munday, H. D. Drew, *Nat. Commun.* **2014**, *5*, 4224; b) T. H. Bointon, I. Khrapach, R. Yakimova, A. V. Shytov, M. F. Craciun, S. Russo, *Nano Lett.* **2014**, *14*, 1751-1755; c) R. Kappera, D. Voiry, S. E. Yalcin, B. Branch, G. Gupta, A. Mohite, M. Chhowalla, *Nat. Mater.* **2014**, *13*, 1128; d) H. Wang, Z. Lu, S. Xu, D. Kong, J. Cha, G. Zheng, P. Hsu, K. Yan, D. Bradshaw, F. B. Prinz, *P. Natl. Acad. Sci. USA* **2013**, *110*, 19701-19706.

[10] a) M. Naguib, M. Kurtoglu, V. Presser, J. Lu, J. Niu, M. Heon, L. Hultman, Y. Gogotsi, M. W. Barsoum, *Adv. Mater.* **2011**, *23*, 4248-4253; b) B. Anasori, M. R. Lukatskaya, Y. Gogotsi, *Nat. Rev. Mater.* **2017**, *2*, 16098.

[11] a) A. Iqbal, F. Shahzad, K. Hantanasirisakul, M. Kim, L. Kwon, J. Hong, H. Kim, D. Kim, Y. Gogotsi, C. Koo, *Science* **2020**, *369*, 446-450; b) X. Tang, X. Guo, W. Wu, G. Wang, *Adv. Energy Mater.* **2018**, 8, 1801897; c) Q. Xue, H. Zhang, M. Zhu, Z. Pei, H. Li, Z. Wang, Y. Huang, Y. Huang, Q. Deng, J. Zhou, *Adv. Mater.* **2017**, *29*, 1604847; d) S. Kim, H. Koh, C. Ren, O. Kwon, K. Maleski, S. Cho, B. Anasori, C. Kim, Y. Choi, J. Kim, *ACS Nano* **2018**, *12*, 986-993; e) J. Nan, X. Guo, J. Xiao, X. Li, W. Chen, W. Wu, H. Liu, Y. Wang, M. Wu, G. Wang; *Small* **2019**, 1902085.

[12] P. Salles, D. Pinto, K. Hantanasirisakul, K. Maleski, C. E. Shuck, Y. Gogotsi, *Adv. Funct. Mater.* **2019**, *29*, 1809223.

[13] X. Wang, T. Mathis, K. Li, Z. Lin, L. Vlcek, T. Torita, N. C. Osti, C. Hatter, P. Urbankowski, A. Sarycheva, M. Tyagi, E. Mamontov, P. Simon, Y. Gogotsi, *Nat. Energy* **2019**, *4*, 241-248.

[14] L. Yang, X. Jiang, W. Ruan, B. Zhao, W. Xu, J. R. Lombardi, *Journal of Raman Spectroscopy* **2009**, *40*, 2004-2008.

[15] A. Dillon, M. Ghidiu, A. Krick, J. Griggs, S. May, Y. Gogotsi, M. W. Barsoum, A. T. Fafarman, *Adv. Funct. Mater.* **2016**, *26*, 4162-4168.

[16] C. Shi, M. Beidaghi, M. Naguib, O. Mashtalir, Y. Gogotsi, S. J. Billinge, *Phys. Rev. Lett.* **2014**, *112*, 125501.

[17] a) J. Wan, S. Lacey, J. Dai, W. Bao, M. Fuhrer, L. Hu, *Chem. Soc. Rev.* **2016**, *45*, 6742-6765; b) N. Jäckel, B. Krüner, K. L. Van Aken, M. Alhabeb, B. Anasori, F. Kaasik, Y. Gogotsi, V. Presser, *ACS Appl. Mater. Inter.* **2016**, *8*, 32089-32093.

[18] Q. Bao, K. Loh, *ACS Nano* **2012**, *6*, 3677-3694.

[19] G. Valurouthu, K. Maleski, N. Kurra, M. Han, K. Hantanasirisakul, A. Sarycheva, Y. Gogotsi, *Nanoscale* **2020**, *12*, 14204-14212.

Entry for the Table of Contents

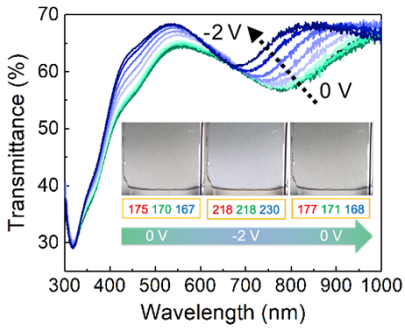

Highly reversible electrochromic performance of semitransparent $Ti_3C_2T_x$ MXene film was realized in organic electrolyte, whose mechanism was revealed by conducting *in-situ* Raman and density functional theory calculation. The interactions between O-termination and the increasing number of Li atoms lead to charge transfer and directly alter the optical excitations, resulting in the color change from dark green to blue.